Flinders
UNIVERSITY

Modelling of flexural behaviour of glass fibre reinforced polymer (GFRP) stobie pole

By Jeongwon Lee

A thesis presented to the Flinders University

Science and Engineering for the Master of Civil Engineering

Supervisor: Aliakbar Gholampour

Author’s Declaration

This work guarantees that no previously submitted materials for any university's degree or diploma are incorporated without acknowledgement and that it does not contain any previously published or prepared materials except for an appropriate reference in the text. This is a real copy of the paper, including the required final revisions, as accepted by the examiners.

I understand that this paper can be provided electronically to the public.

Signed: Jeongwon Lee

Date: 03/11/2021

Acknowledgements

Above all, I would like to thank my supervisor Dr Aliakbar Gholampour for helping me a lot. While working on the project for a year, there were many difficulties, but he always gave me a lot of advice and help, so I was able to finish this project. Also, I would like to express my gratitude to all professors at Civil Engineering.

I would like to express my infinite gratitude to Flinders University for laying the foundation for becoming an engineer through high-quality lectures. I also thank the friends of Civil Engineering for their great help and support in similar situations.

Lastly, I would like to express my apologies and gratitude to my family for always understanding and supporting me during my busy and difficult year.

Executive Summary

In South Australia, steel is the most important and common material used for stobie poles. However, the steel beam exposed to the outside is prone to corrosion, which can greatly reduce its lifespan.

Experimental tests have already been conducted on materials that can replace the steel of stobie pole. However, experimental testing is a time-consuming and expensive process, especially to investigate the various properties, sizes, and effects of material parameters.

Therefore, the research objective of this project is to prove its validation of the results from the experimental test by simulating the behaviour of the stobie pole models using the finite element method (FEM). This can overcome disadvantages (cost and time consumption) related to the experimental test.

ABAQUS software was used to model the nonlinear behaviour of composite materials and materials such as stobie poles using nonlinear FEM. The specimens in the experimental test were modelled under the same conditions and the results were compared.

As a result, the error range of the stiffness was between about 10-20% and the overall average was approximately 16%. Validation of modelling can be confirmed through the normal distribution and standard deviation of errors. The standard deviation of the weak axis was confirmed to be 5.89, and the standard deviation of the strong axis was 2.18.

Contents

List of Tables / Figures

1 Introduction

A stobie pole, made of two steel supports held apart by a concrete slab, was invented by James, an engineer at Adelaide Electric Supply Company. Stobie pole used materials that were easily available because of the lack of wood that was suitably long, sturdy and resistant to termites suitable for South Australia.

In South Australia, steel is the most important and common material used for stobie poles. However, steel has several problems. The steel stobie pole exposed to the outside can significantly reduce its lifespan because corrosion easily occurs. On average, the lifespan of the stobie pole is expected to be 20-30 years, but corrosion damage begins to appear after 10 years approximately. One of the various methods to prevent corrosion of steel is to coat the surface of the steel exposed to the outside. But, since the maintenance costs used to prevent corrosion are significantly high, it is not economically reasonable to repair the stobie pole to maintain its maximum life. Although maintaining a stobie pole is expensive, it is still a widely used reality because there is still no proper solution. Recently, a lot of studies have actively researched materials to replace steel that consumes high maintenance costs. Among the various materials, the most attractive attention material is the fibre-reinforced polymer (FRP) which have improved proper performance and durability. Fibre Reinforced Polymers are used in various fields and studies have demonstrated that material properties are suitable for replacing steel and resistant to corrosion. (Gilbert Nkurunziza et al., 2005)

Experimental testing for the stobie pole has already been performed before. Nevertheless, experimental testing is a time-consuming and expensive process, especially to test the various size, properties and effects of parameters of materials. Thus, the way to overcome the disadvantages (cost and time-consuming) related to experimental tests by simulating the trend of changes in various variables is to use the finite element method (FEM). Non-linear FEMs can be used to model the nonlinear behaviour of composite materials and materials such as stobie poles. Although there are many commercial 3D FEM packages to analyse composite material behaviour, ABAQUS was used in this study. ABAQUS is an application software used for both the analysis and modelling of composite material structures such as the stobie pole, and also visualizing and assemblies the FE analysis result. (Aboubieda Alamin et al., 2016)

Today, material simulation is often being performed by engineering groups using simulation tools. The ABAQUS offers powerful and complete solutions for both routine and sophisticated engineering problems covering a vast spectrum of industrial applications. To verify the simulated models for stobie poles replaced with glass fibre reinforced polymer (GFRP) in steel, the results of the simulation were validated with experimental data reported by Xinyuan Zhang (2020).

1.1 Research Aim

Since the steel of the stobie pole is a material with corrosion problems, epoxy coating is required to extend the life-span, and high costs are incurred to maintain the life of the stobie pole. It is important to find an appropriate material that can replace steel and the performance of the material should be checked through the experimental tests. However, each experiment on various materials, dimensions and parameters also takes a lot of money and time. Therefore, modelling using the software can save time and money and identify the behaviour of materials.

The primary research aim in this project is to develop the ABAQUS models that present the load-displacement performance and stiffness behaviour of the GFRP stobie pole that have replaced steel. At the conclusion, the finite element models will be compared and validated with the experimental results.

1.2 Research Significance

FEA (Finite element analysis) is a widely used and important technique in various industries. Since testing a specimen of an actually built structure incurs a lot of time and high cost, simulation using finite element analysis can reduce the cost.

In particular, the ABAQUS package is a good program to test the reactions of various materials in specific environments such as heat, pressure, gravity, and load. It is possible to perform more additional simulations on the stobie pole by verifying its validity through comparison between the experimental value of the GFRP stobie pole and the simulation result. Ultimately, it can save time and money and develop engineering better items.

1.3 Organization

• Chapter 1: Introduction

• Chapter 2: Literature Review

• Chapter 3: Methodology of Finite Element Model

• Chapter 4: Simulating Result

• Chapter 5: Data Analysis and Validation

• Chapter 6: Conclusion

• Chapter 7: Recommendations & Future work

2 Literature Review

2.1 Significant issues of Steel Reinforced Concrete

In reality, many reinforced concrete structures are exposed to poor conditions, so it is unlikely that they will reach the maximum life of the structure due to durability problems. The main cause of weakening reinforced concrete structures is often corrosion due to carbonation or chloride. Therefore, many countries spend a lot to prevent the corrosion of structures. More than 41% of all bridges and multi-layer parking lots that are more than 40 years old are estimated to be structurally insufficient, because of de-icing salts and corrosion caused by severe climates in Canada. In the United States, more than 40% of the bridges inspected were classified as functionally or structurally defective. This defect was due to damage caused by corrosion of steel and a significant increase in traffic load over a long period of time. Therefore, many bridges are subject to higher loads than the design limitations designed in the past, and some endure twice as much loads.

Maintaining and repairing the corrosion of steel in reinforced concrete structures requires a lot of repair costs. The United States spends $50 billion to $100 billion annually to repair multi-layered parking lots, and Canada is estimated to spend $6 billion. Therefore, new technologies are being developed to reduce corrosion of reinforcement and prevent economic losses. Some of the developed technologies include epoxy coating and galvanizing steel bar,

and others have developed a technology called cathodic protection. So far, epoxy-coated steel has accounted for 15% of the steel market in North America. Various technologies have been developed, but it was impossible to completely prevent corrosion. Therefore, research on the development of a reinforced new material such as a fibre-reinforced polymer (FRP) is actively underway. (Gilbert Nkurunziza et al., 2005)

2.2 Glass Fibre Reinforced Polymer (GFRP)

In hybrid concrete-GFRP structural elements, the substitute use of GFRP pultruded profiles demonstrates a very interesting potential for rehabilitation or new structures. In fact, there are some structural benefits in connecting the GFRP pultruded profile to concrete compression elements, such as an increase in flexural rigidity & strength capacity of the structure, and a decrease in a structural deformation. This makes more effective use of the GFRP profile and prevents buckling. (Joa˜o R. Correia et al., 2007)

An initial experiment on concrete-GFRP elements was developed in rehabilitation solutions. In this experiment, it was proved that the effective way for the strengthening of reinforced concrete structural elements was the bonding of GFRP laminate. Some advantages of the solution are that it is easy to use compared to the use of steel plates and has high resistance to corrosion and light self-weight. When it comes to regenerative use of CFRP bonding systems, GFRP solutions have the advantage of lower costs although it has much less stiffness. (Joa˜o R. Correia et al., 2007)

FRP composite materials with advantages of high specific strength and coefficient have long been used in various fields. Due to the stiffness and strength of the composite build up that varies depending on the orientation sequence of the plies, the layer direction of the fibre-reinforced polymer composite material should be developed according to the strength and stiffness. Fibres running in one direction are unidirectional materials. In addition, strength and stiffness exist in the direction of fibre only. However, the strength and stiffness of the fibre flowing in both directions move in both directions of the fibre. (Meltem Altin Karatas et al., 2018)

Image removed due to copyright restriction.

Figure 1. Fibre Reinforced Polymer orientation types (Meltem Altin Karatas, 2018)

2.3 Advantages and Disadvantage of Using GFRP over Steel

2.3.1 Advantages

The glass fibre reinforced polymer (GFRP) pultruded profiles, which can be used as a construction material, has great potential. GFRP pultruded profiles has various advantages related to low self-weight, weight ratio, and electromagnetic transparency compared to traditional materials. It also has the advantage of easy installation and improved durability, reducing maintenance costs. (Joa˜o R. Correia et al., 2007)

One of the causes of significantly reducing the durability in reinforced concrete structures is corrosion in steel. Therefore, in order to prevent corrosion of the steel, a method of replacing the reinforcing bar with fibre reinforced plastic polymer (FRP) bars can be used as an effective method. In general, high-strength FRP has been widely applied to steel structures or concrete structures as structure reinforcements. (Sanfeng Liu et al., 2019)

2.3.2 Disadvantages

The elastic modulus of the fibre reinforced polymer (FRP) bars are smaller than that of the steel bars. Therefore, the FRP reinforced bar has the advantage of longer elastic deformation before they fail, but it can cause fatal damage to structures because it is easier to rupture than

steel. On the other hand, steel has a large fracture strain, but the yield strength is not high because the elastic deformation step is too short. (Sanfeng Liu et al., 2019)

When the elastic modulus is low, it becomes a structural design usually controlled by instability and deformability, not strength limitation. In addition, the low elasticity-shear modulus ratio leads to a critical contribution to the shear of the overall deformation, in particular in the less slender beams. This aspect such as limited use related to the ultimate strength of the material or the high cost of these factors can explain the fact that the use of FRP materials when constructing new structures is limited to several pilot projects. (Joa˜o R. Correia et al., 2005)

2.4 Application of GFRP in Civil Engineering

The glass fibre reinforced polymer (GFRP), a new material that has excellent properties such as corrosion resistance, high mechanical properties, and light weight, has attracted a lot of attention worldwide and various studies are being conducted. Through many international conferences, research conducted by various institutes of research was announced and the acquired knowledge was shared. Around the world, the GFRP bar has been used as primary reinforcement in many bridges. GFRP bar consists of thousands of fibres and resins with a diameter of 15 μm approximately. In general, GFRP bars are manufactured by a pultrusion process. There are already many highway bridges that GFRP bars have been used as primary reinforcements in Canada. The bridge consists of a concrete deck slab of 200 mm thick supported by 4 steel girders. In addition, GFRP was used as a reinforcement in the longitudinal and transverse directions of slabs and barriers. (Gilbert Nkurunziza et al., 2005)

GFRP (Glass fibre reinforced polymer) composites, which have superior properties compared to the properties of traditional materials, are increasingly used in various structures such as buildings and bridges. In particular, the most commonly used material in civil construction is pultruded profiles. A typical pultruded GFRP similar to the cross-sectional of steel forms bridge decks using adhesive bonding. Nowadays, pultruded GFRP profiles are usually used to build bridges for decks of vehicles or pedestrian bridges. Cable-stayed or truss systems are applied for the pedestrian bridges to acquire bigger spans because the span of the beams and

the height of cross-sectional is limited. This system applies to the anisotropic properties of the profile, and the reason is that it works less in bending & shear and in axial compression & axial. The profiles acting as one-way slabs in the bridge deck are generally arranged in the transverse direction. (Thomas Kellerc et al., 2015)

Image removed due to copyright restriction.

Figure 2. Typical GFRP profiles & GFRP bridge deck system (Thomas Kellerc, 2015)

2.5 Experimental Research on GFRP stobie pole

The experimental test has presented that there is a huge gap in the behaviour between the GFRP stobie pole and steel stobie pole specimens, but the GFRP stobie pole specimens have improved the behavioural performance by installing the internal reinforcements. So, the GFRP stobie pole is getting close to the strain performance of steel.

According to the experimental test results, it was proved that the size of concrete had a slight impact on the displacement and strain for the applied load firstly. There was only an 8% increase in the stiffness when the size is getting bigger from 75 mm to 125 mm.

Secondly, it can be seen that the steel specimen has higher stiffness than the GFRP specimens. However, GFRP specimens have the modulus of 12-60 GPa and steel specimens have the modulus of 200 GPa which is approximately 17 times higher, while experimental results show 3-7 times higher stiffness performance.

Thirdly, the GFRP I beam stobie pole presented better performance than the C beam stobie pole as it has increased 200% stiffness in the loading case of the weak axis. And also, it has increased by 40% stiffness in the loading case of the strong axis.

Fourthly, a value with 82% higher stiffness than normal GFRP specimens on the weak axis was obtained from the internally reinforced GFRP specimens. On the strong axis, 60% higher stiffness than normal GFRP specimens was obtained.

The experimental test in this project has shown that the glass fibre reinforced poly (GFRP) can be a good substitute material for replacing the steel of the stobie pole in the future. (Xinyuan Zhang, 2020)

Table 1. Stiffness results in weak & strong axis of Group 1, 2, 3 (Xinyuan Zhang, 2020)

Table removed due to copyright restriction.

2.6 Research Gap

The stobie pole's steel is exposed to poor environments, so durability problems are constantly being discussed. Therefore, new materials were needed to complement for these shortcomings, and GFRP showed interesting potential as an alternative material.

However, various experiments are still actively underway because it still requires a lot of verification. The problem is the cost and time incurred to conduct the experiment. The performance of the material can be easily confirmed through simulation through small analysis.

Based on the literature review, to date. There is no study to model GFRP reinforced concrete beams. Therefore, this study presents the first results on FEM of GFRP reinforced concrete beams. The results are compared with the experimental results for validation.

3 Methodology of Finite Element Model

The Finite Element (FE) modelling can analyse the structural behaviour of a model to which various load cases and materials are applied. Therefore, this modelling has been widely used because of its high efficiency and reasonable accuracy. The most reliable method is the results obtained through the experimental tests in practice. However, there is a disadvantage in that it requires the high cost to conduct experimental tests and takes long preparation and test time. An advanced interface model has been used between GFRP beam and concrete of stobie pole in ABAQUS. Through the ABAQUS package that a finite element program extensively used in civil engineering, various components (GFRP, concrete and steel) can be simulated and compared with experimental results

This chapter explains the methodology of the model. In ABAQUS, the modelling process proceeds in the order of geometry, property, assembly, interaction, load, boundary condition and meshing.

3.1 Specimen geometry

3.1.1 Concrete & GFRP C Beam

All specimens of the stobie pole are 1580 mm long and consist of a total of 9 specimens. In those specimens, the six models will consist of GFRP C beam, and the other three models will consist of steel C beam. As can be seen in the table 2, the heights of the two materials are the same at 100 mm, but the flange lengths of steel and GFRP are 50 mm and 30 mm, respectively.

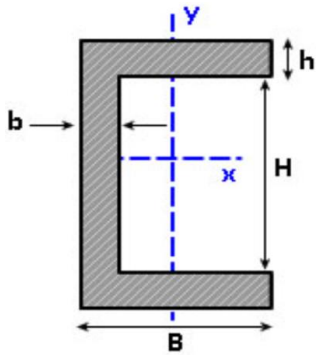

Figure 3. Cross-section of C beam

Table 2. Parameters of C beam (GFRP & Steel) (Unit : mm)

C-section	B	b	H	h
GFRP	30	6	88	6
Steel	50	6.7	91.6	4.2

3.1.2 Concrete & GFRP Reinforcing bar

In this project, three types of concrete were used. Although all heights are the same 100 mm, such as C beam, samples were made of concrete with a width of 75 mm, 100 mm and 125 mm to test the performance according to the width of the concrete. In addition, another specimen group was created to test the GFRP reinforcing bar as well as the comparison of materials between the GFRP beam and steel beam. GFRP reinforcing bar with a diameter of 10mm and 20mm was used in this group.

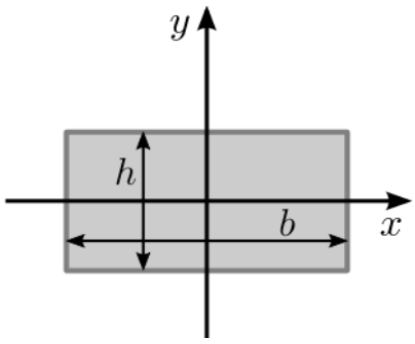

Figure 4. Cross-section of concrete

Table 3. Parameters of concrete (Unit : mm)

	Concrete A	Concrete B	Concrete C
H x B	100 x 75	100 x 100	100 x 125

3.1.3 Specimens for Group 1, 2 & 3

A total of 9 specimens were prepared based on the materials described above and classified into three large groups according to the criteria. In the first group, as shown in figure 5 below, two GFRP C beams were used on both sides of the concrete for each of the three specimens, and the sizes of the concrete consisted of 100 mm*75 mm, 100 mm*100 mm and 100 mm*125mm. Therefore, the overall widths are 135 mm, 160 mm, and 185 mm, respectively.

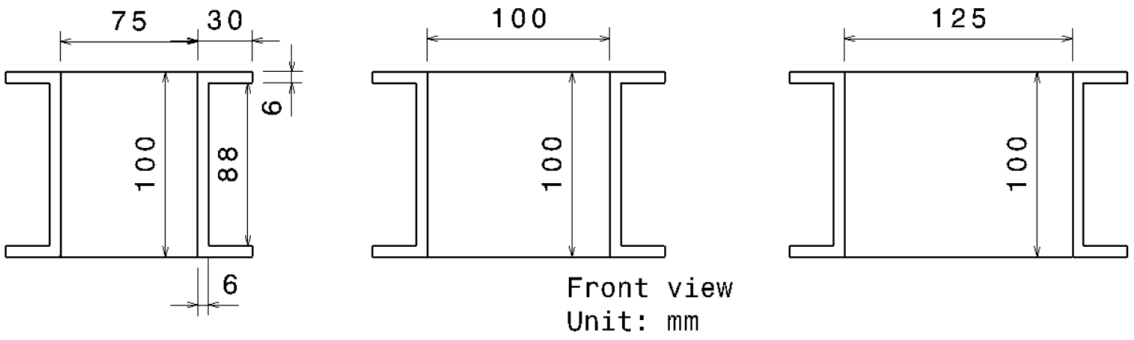

Figure 5. Group 1 - GFRP C-section & Concrete Beam

The second group consisted of the same form as the first group. Here, instead of using the GFRP C beam, the specimens were made with the steel C beam. And just like group 1, the size of the concrete consisted of 100 mm*75 mm, 100 mm*100 mm and 100 mm*125mm. Therefore, as shown in figure 6, the overall widths are 175 mm, 200 mm, and 225 mm, respectively.

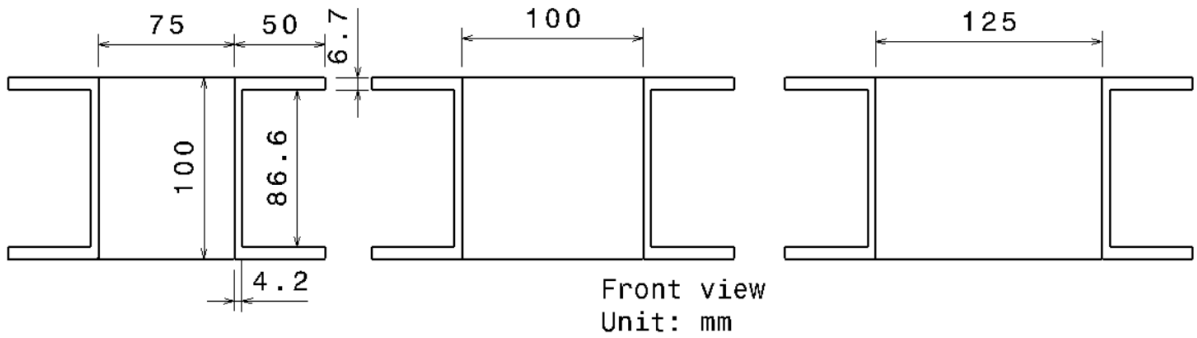

Figure 6. Group 2 - Steel C-section & Concrete Beam

In this way, group 1 and group 2 described above consisted of different materials of GFRP and steel C beam at the concrete of the same size. This is to compare the behaviour of the two materials (GFRP, Steel).

Finally, the third group is a group for testing a slightly different type of sample unlike group 1 and group 2. As shown in figure 7 below, the back of the two GFRP C beams was attached to each other to make it a beam of I shape. In addition, two samples composed of two GFRP beams were added with GFRP reinforcing bars of different diameters (10 mm, 20 mm), and all covers were made with 20 mm. The width of the concrete in this group is constant at 100 mm.

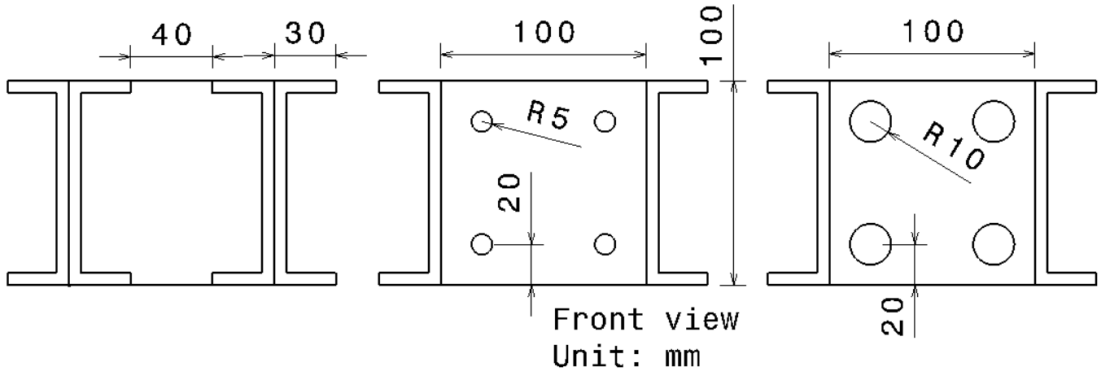

Figure 7. Group 3 - Double C-section & Concrete Beam with rebars

3.2 Material properties

The most important thing for modelling is to understand the exact properties of the material. In particular, since it is a project to simulate real behaviour, the properties of the materials used in the experimental test must be accurately entered. There are three main materials used in this study: GFRP, concrete and steel.

3.2.1 Concrete

Concrete is a composite material composed of various materials. These include fine aggregates, coarse aggregates, cement and water. Various methods have been used to model the behaviour of concrete in programs. Among them, CDP is a method of dealing with compressive crushing and tensile cracking of concrete. Therefore, CDP was used to simulate the behaviour of concrete for FE modelling.

- CDP (Concrete Damaged Plasticity)

The CDP considering compressive crushing and tensile cracking uses five parameters priorly. There are the flow potential eccentricity, dilation angle (ψ), viscosity parameter (μ), the ratio f_{bo}/f_{c0} of biaxial compressive yield stress to uniaxial compressive yield stress, the ratio K of the second stress invariant on the tensile meridian to that on the compressive meridian. (Joseph George, 2015)

Table 4. Plastic damage parameters

Parameter	Value or Type
Dilation Angle (ψ)	31
Eccentricity	0.1
f_{bo}/f_{c0}	1.16
Viscosity Parameter (μ)	0.001
K	0.667

- Compression & Tensile Model

The test for concrete material properties, including tensile strength, elastic modulus and compressive strength test, were performed over 28 days in the experimental test before. Therefore, as shown in table 5, average compressive strength, tensile strength, and elastic modulus can be confirmed.

Table 5. Concrete properties for 3 groups (Xinyuan Zhang, 2020)

28 Day results		Compressive test (MPa)		Tensile test (MPa)		Elastic modulus (GPa)
Group 1 GFRP	1	31.76	1	4.66	1	24.27
	2	30.96	2	4.78	2	23.98
	3	29.97				
Average		30.90		4.72		24.13
28 Day results		Compressive test (MPa)		Tensile test (MPa)		Elastic modulus (GPa)
Group 2 Steel	1	29.97	1	4.58	1	23.56
	2	30.26	2	4.64	2	24.75
	3	30.92				
Average		30.38		4.61		24.16
28 Day results		Compressive test (MPa)		Tensile test (MPa)		Elastic modulus (GPa)
Group 3 GFRP	1	32.52	1	4.64	1	26.83
	2	32.54	2	4.86	2	24.05
	3	32.67				
Average		32.58		4.75		25.44

3.2.2 Steel beam

The material properties of steel required to be entered into the program are Poisson's Ratio ($\boldsymbol{\nu}$), Yield Stress ($\boldsymbol{f's}$) and Modulus of Elasticity ($\boldsymbol{Es}$). The steel beam used in the experimental test is 100*50 black channel C steel beam AS3679/300 (100 PFC) which has a modulus of 200 GPa. Furthermore, yield stress can be obtained according to standard AS/NZS 3679.1:2016.

Table 6. Material properties of steel

Parameter	Value or Type
Modulus of Elasticity ($\boldsymbol{Es}$)	200 [GPa]
Poisson's Ratio ($\boldsymbol{\nu}$)	0.3
Yield Stress ($\boldsymbol{f's}$)	360 [MPa]

Table 7. Tensile test requirements for flats and sections (AS/NZS 3679.1:2016)

Grade	Minimum yield stress, (R_{eH}) MPa (see Note 1)				Minimum tensile strength (R_m)	Minimum elongation on a gauge length of $5.65\sqrt{S_o}$ (see Note 4)
	Thickness, mm (see Note 3)					
	<11	≥11 and ≤17	>17 and <40	≥40	MPa	%
300, 300L0	320	300	280	280	440	22
300L15, 300S0	320	300	280	280	440	25 (see Note 2)
350, 350L0	360	340	340	330	480	20
350S0, 350L15	360	340	340	330	480	25 (see Note 2)

3.2.3 GFRP beam & reinforcing bar

The materials used in the experimental test were V-rod GFRP C beam and rebar. As shown in tables 8 and 9 provided by V-rod Australia, the properties of the material (Modulus of Elasticity, Guaranteed Tensile Strength, Tensile Strain etc..) can be confirmed according to the size of the material.

Table 8. GFRP C beam properties (V-Rod, 2019)

Properties	Standard	Unit/Value	Required	Observed
Tensile Strength	ASTM D638	Mpa	Min 207.000	370.000
Flexural Strength	ASTM D790	Mpa	Min 207.000	375.000
Flexural Modulus	ASTM D790	Mpa x 10^4	Min 1.000	1.200
Izod Impact	ASTM D256	Kj/M^2	Min 100.000	149.000
Compressive Strength	ASTM D695	Mpa	Min 207.000	345.000
Compressive Modulus	ASTM D695	Mpa x 10^4	Min 1.000	1.823
Barcol Hardness	ASTM D2583	-------	Min 50.000	55.000
Glass Content	ASTM D2584	%	Min 45.000	65.000
Water Absorption (%) after 30 min immersion in water at 23 °	ASTM D570	%	Max 0.600	0.100
Oxygen Index	IS 13410	%	Min 24.000	28.000
Volume Resistivity	IS 13410	ohm - cm	1 x 10^{14}	Passed
Surface Resistivity (24 h in water)	IS 13410	Ohm	1 x 10^{18}	Passed
Di electrical Strength Axial	ASTM D149	KV/25 mm	30 - 45	Passed
Di electrical Strength Radial	ASTM D149	KV/25 mm	10 - 15	Passed
Smoke Development	BS-476 Part 5	-------	Max 450	400
Flame Spread Index	BS-476 Part 6	-------	0-15	10
Flame Spread at 1.5 min Class 1	BS-476 Part 7	mm	165 (+25)	100

Table 9. GFRP bar properties (V-Rod, 2019)

		#3 (10M)	#4 (12M)	#5 (15M)	#6 (20M)	#8 (25M)
Guaranteed tensile strength (ASTM D7205)	MPa	1100	1100	1100	1100	1100
	ksi	159.5	159.5	159.5	159.5	159.5
Minimum tensile modulus (ASTM D7205)	GPa	60				
	ksi	8702.3				
Guaranteed transverse shear capacity (ASTM D7617)	MPa	180				
	ksi	26.1				
Resin		Vinylester				
Weight	g/m	175	310	442	633	1127
	lb/ft	0.118	0.208	0.297	0.425	0.757
Effective cross-sectional area (including sand coating)	mm^2	83.8	145	232.9	326.8	572.3
	in^2	0.130	0.225	0.361	0.507	0.887
Effective diameter	mm	10.33	13.59	17.22	20.39	26.99
	in	0.407	0.535	0.678	0.803	1.063
Nominal cross-sectional area (CSA S807 Table 1)	mm^2	71	129	199	284	510
	mm^2	0.110	0.199	0.308	0.440	0.790

Table 10. Material properties of GFRP C beam and rebar

Parameter	Value or Type	
	C beam	Rebar
Modulus of Elasticity	12 GPa	60 GPa
Guaranteed Tensile Strength	370 MPa	1100 MPa
Tensile Strain	1.59 %	1.59 %

3.3 Boundary Condition & Load cases

Boundary conditions and 2 different load cases were applied under the same conditions as the experimental test for modelling. Two rollers were installed at both ends of the bottom of the specimen to support. In addition, a roller capable of applying a load was installed in the middle of the upper side of the specimen. Since the two rollers at the bottom should not move in all directions, ENCASTRE (U1 = U2 = U3 = UR1 = UR2 = UR3 = 0) was set through boundary condition.

The load was applied to the top roller. As shown in figure 8 below, 4 kN was applied when a load was applied directly to concrete (Weak axis), and 5 kN was applied when a load was applied to C beam (Strong axis).

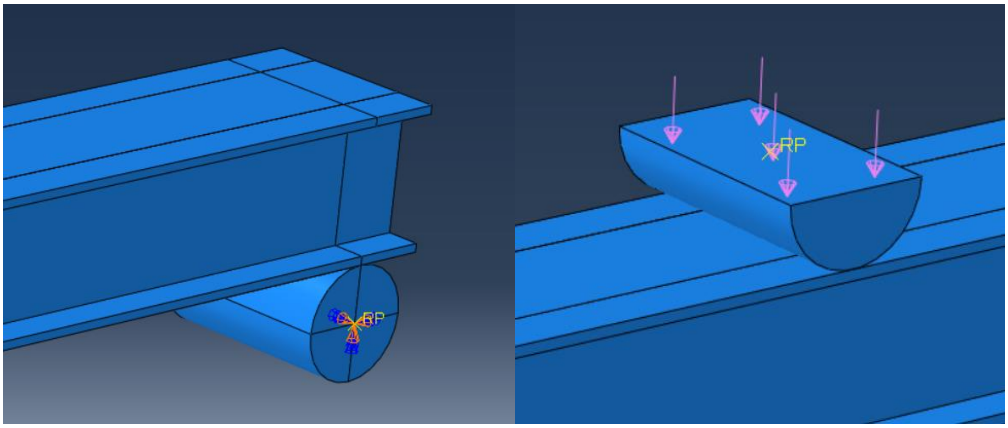

Figure 8. Boundary condition & loading in ABAQUS

Image removed due to copyright restriction.

Figure 9. Load cases: Weak & Strong axis (Xinyuan Zhang, 2020)

3.4 Assembly & Meshing

Each part (Concrete, steel or GFRP C beam, rebar and support) produced were assembled to make the model under the same conditions as the physical model. This assembly interface allows creating of a finite element meshing. More detailed simulation results can be obtained through meshing. Since the ABAQUS program used in this thesis is a student edition, the number of nodes allowed was limited to 1000. Therefore, the approximate global sizes of the concrete and the C beam were 70 and 50, respectively.

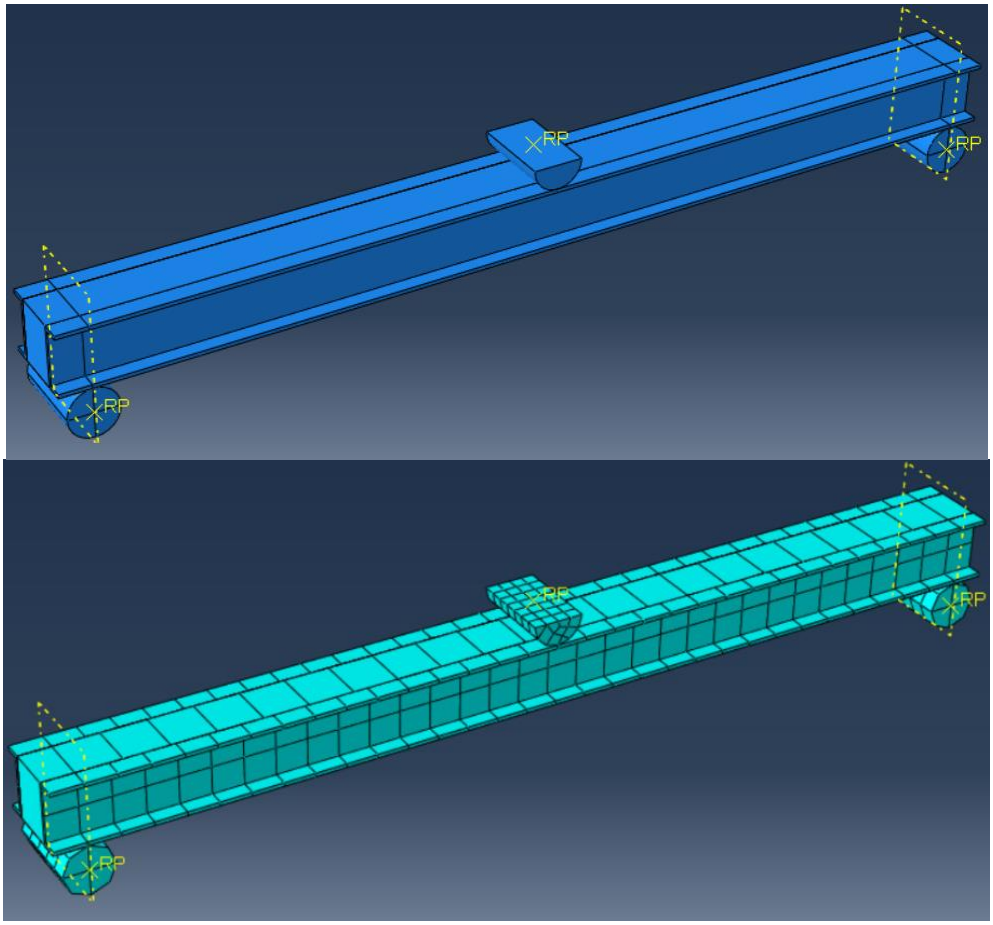

Figure 10. Assembly & Meshing of model in ABAQUS

4 Simulating Result

This chapter presents the results of FE modelling using ABAQUS. A total of 9 models in 3 groups were analysed. The load-displacement behaviour will be presented in different two load cases (weak & strong axis) and the stiffness of the specimen will be determined. Therefore, all result values determine the accuracy of FE modelling by comparing them with the result of the experimental test. The errors in the Experimental & Simulating test are expected to cause some differences between the two results.

4.1 Modelling behaviour on weak axis

4.1.1 Result for Group 1

The result for Group 1 presents load-displacement graphs when a load of 4 kN is applied to three types of models (75 mm, 100 mm & 125 mm of concrete and GFRP C beam) on the weak-axis.

The maximum displacement of the 75mm concrete specimen was 4.93mm and the slope was 0.1724. The displacement of the experimental test is approximately 5.5 mm, and the error between the two values is approximately 10.2%.

Second, the 100 mm concrete specimen presents a maximum displacement of 4.7 and a slope of 0.1701. In addition, the displacement was 5.7mm in the experimental test, and the error with the modelling result was calculated as 16.99%.

Finally, the concrete specimen with a width of 125 mm was measured with a maximum displacement of 3.75 mm, and the slope was 0.2105. The experimental displacement value is 4.2 mm, indicating an error of 10.43%.

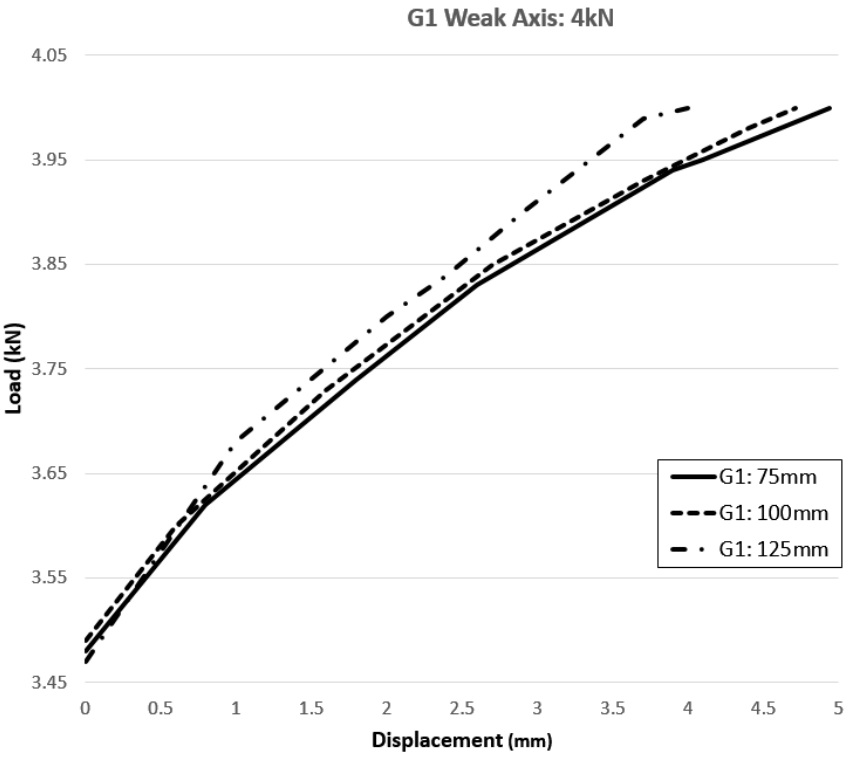

Figure 11. Modelling results: Load-Displacement behaviour of Group 1 on weak axis (4 kN)

4.1.2 Result for Group 2

As for group 2 on the weak axis, concrete specimens 75mm, 100mm, and 125mm, such as group 1, are applied. Steel C beam was attached to this concrete beam in place of GFRP.

The maximum displacement of the 75mm concrete specimen was 1.59 mm and the slope was 0.63. The experimental value is approximately 1.8 mm, and the error between the two values is approximately 10.43%.

Second, the maximum displacement of the 100 mm concrete specimen was 1.49 mm and the slope was 0.7732. The displacement of the experimental test is approximately 1.7 mm, and the error between the two values is approximately 10.1%.

Third, the concrete specimen with a width of 125 mm was measured with a maximum displacement of 1.38 mm, and the slope was 0.6284. The displacement experiment value of this specimen is 1.6 mm, indicating an error of 13.14%.

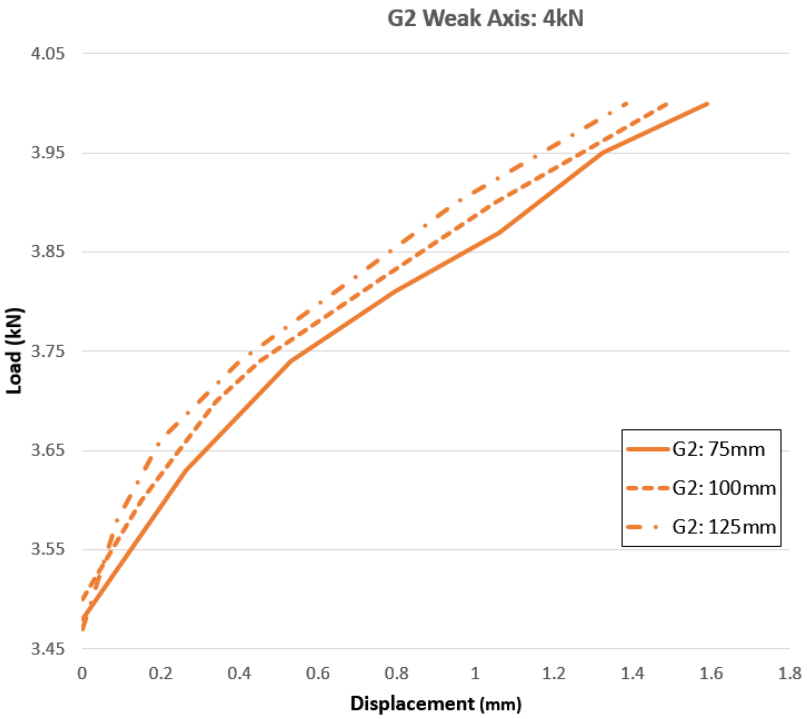

Figure 12. Modelling results: Load-Displacement behaviour of Group 2 on weak axis (4 kN)

4.1.3 Result for Group 3

Finally, group 3 on the weak axis presents the behaviour of the specimen consisting of GFRP I beam and reinforcing bar, unlike previous groups.

The first is a specimen of GFRP C beam used in group 1 attached to 100 mm concrete with GFRP rebar of a diameter of 10 mm. As a result of the modelling analysis, the maximum displacement was 3.63 mm and the slope was 0.3862. The maximum displacement of the experimental value was 4.4 mm and the error was calculated as 16.8%.

The second is a specimen in which the diameter of the GFRP rebar in the first specimen is increased to 20 mm. The maximum displacement is 2.55mm and the slope is 0.32999, and the displacement experiment value is 2.9mm, which shows an error of 13.55%.

Third, the maximum displacement of the sample with GFR I beam attached to both sides of the 100 mm width concrete was 2.19 mm and the slope was 0.32. The displacement experiment value is approximately 2.8 mm, and the error between the two values is 23%.

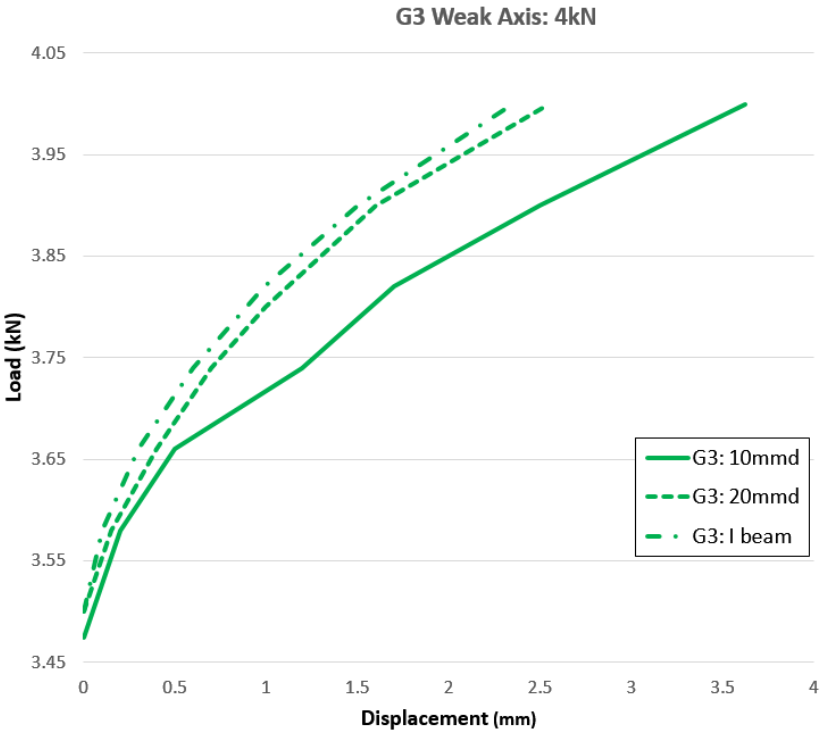

Figure 13. Modelling results: Load-Displacement behaviour of Group 3 on weak axis (4 kN)

In this way, the modelling result of specimens on the weak axis was confirmed. The maximum displacement of the modelling can be analysed compared to the displacement of the experimental test. The load-displacement behaviour of the experimental test results can be found in the appendix.

As a result, the difference between the modelling results of Groups 1, 2, and 3 and the experimental results can be confirmed through the table 11 below. In Group 1, the average error of displacement was presented to be 12.52%, and the average error of Group 2 and Group 3 was 11.22% and 17.78%, respectively.

Table 11. The value of Load-Displacement behaviour with difference on weak axis

	GFRP (G1)			Steel (G2)			Double-GFRP (G3)		
Weak axis [4 kN]	75mm	100mm	125mm	75mm	100mm	125mm	10mmd	20mmd	I beam
Displacement Experiment [mm]	5.5	5.7	4.2	1.8	1.7	1.6	4.4	2.9	2.8
Displacement Modelling [mm]	4.93	4.70	3.75	1.59	1.49	1.38	3.63	2.55	2.19
Error [mm]	0.56	0.96	0.43	0.18	0.17	0.21	0.73	0.40	0.65
Error [%]	10.21	16.99	10.36	10.43	10.10	13.14	16.80	13.55	23.00

4.2 Modelling behaviour on strong axis

4.2.1 Result for Group 1

The result for Group 1 presents load-displacement graphs when 5 kN is applied to the three specimens (75 mm, 100 mm & 125 mm of concrete and GFRP C beam) on the strong-axis.

The maximum displacement of the 75mm concrete specimen was 10.43mm and the slope was 0.19. The displacement of the experimental test is approximately 12.2 mm, and the error between the two values is approximately 14.44%.

Second, the 100 mm concrete specimen presents a maximum displacement of 7.85 and a slope of 0.3. In addition, the displacement was 9.3 mm in the experimental test, and the error with the modelling result was calculated as 15.57%.

Finally, the concrete specimen with a width of 125 mm was measured with a maximum displacement of 6.24 mm, and the slope was 0.38. The displacement experiment value is 7 mm, indicating an error of 11.26%.

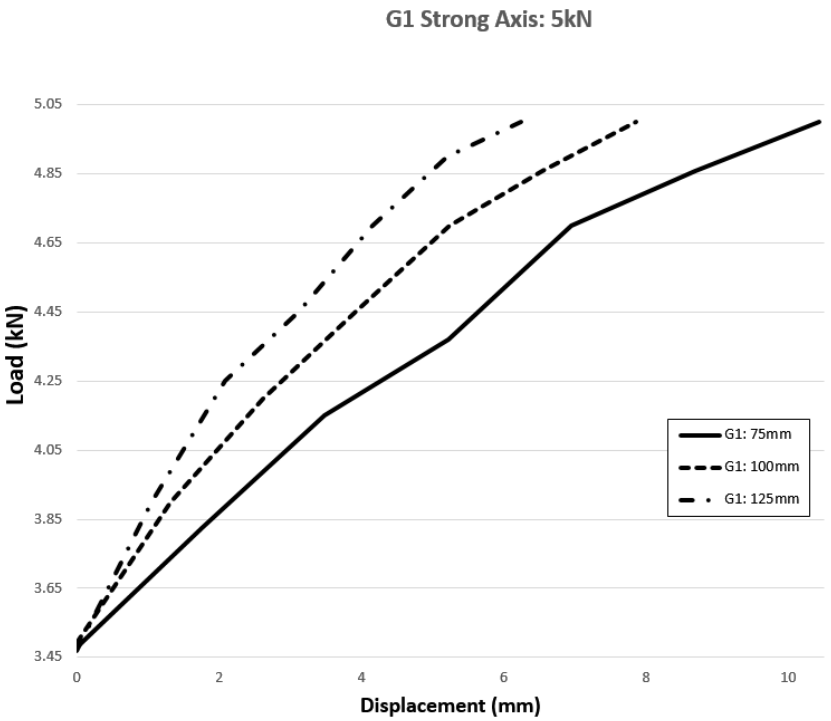

Figure 14. Modelling results: Load-Displacement behaviour of Group 1 on strong axis (5 kN)

4.2.2 Result for Group 2

The specimen such as 4.1.2 Result for Group 2 was converted into strong axis and modelled.

The maximum displacement of the 75mm concrete specimen was 2.87 mm and the slope was 1.18. The experimental value is approximately 3.4 mm, and the error between the two values is approximately 14.85%.

Second, the maximum displacement of the 100 mm concrete specimen was 2.44 mm and the slope was 1.1. The displacement of the experimental test is approximately 1.2 mm, and the error between the two values is approximately 99.34%.

Third, the concrete specimen with a width of 125 mm was measured with a maximum displacement of 1.78 mm, and the slope was 1.24. The displacement experiment value of this specimen is 2.1 mm, indicating an error of 14.78%.

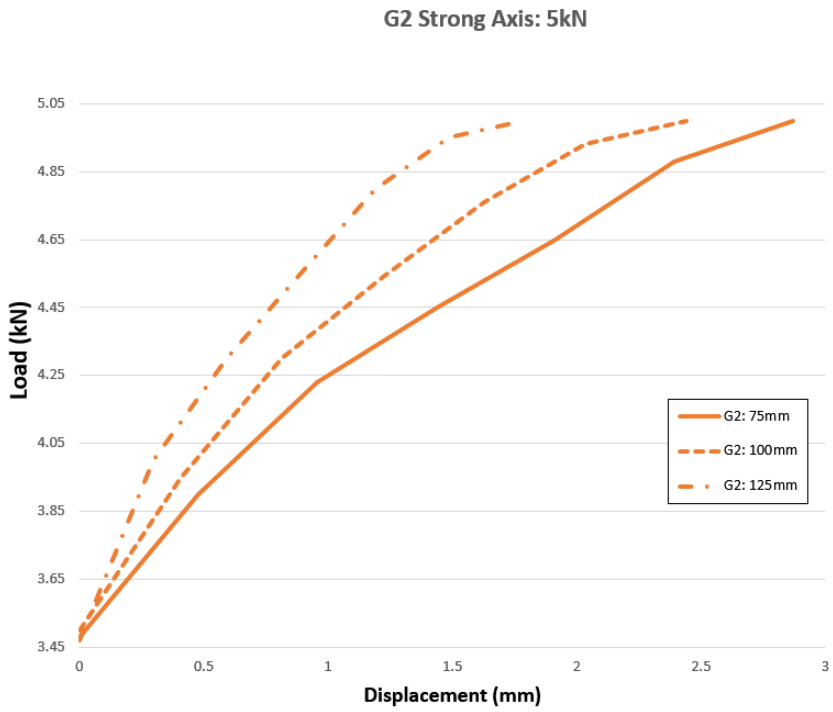

Figure 15. Modelling results: Load-Displacement behaviour of Group 2 on strong axis (5 kN)

4.2.3 Result for Group 3

Three specimens were modelled on the a-axis. The first is a specimen of GFRP C beam used in group 1 attached to 100 mm concrete with GFRP rebar of a diameter of 10 mm. As a result of the modelling analysis, the maximum displacement was 7.34 mm and the slope was 0.41. The maximum displacement of the experimental value was 8.7 mm and the error was calculated as 15.36%.

The second is a specimen in which the diameter of the GFRP rebar in the first specimen is increased to 20 mm. The maximum displacement is 6.78 mm and the slope is 0.48, and the displacement experiment value is 7.7 mm, which shows an error of 12.05%.

Third, the maximum displacement of the sample with GFR I beam attached to both sides of the 100 mm width concrete was 5.23 mm and the slope was 0.46. The displacement experiment value is approximately 5.9 mm, and the error between the two values is 11.85%.

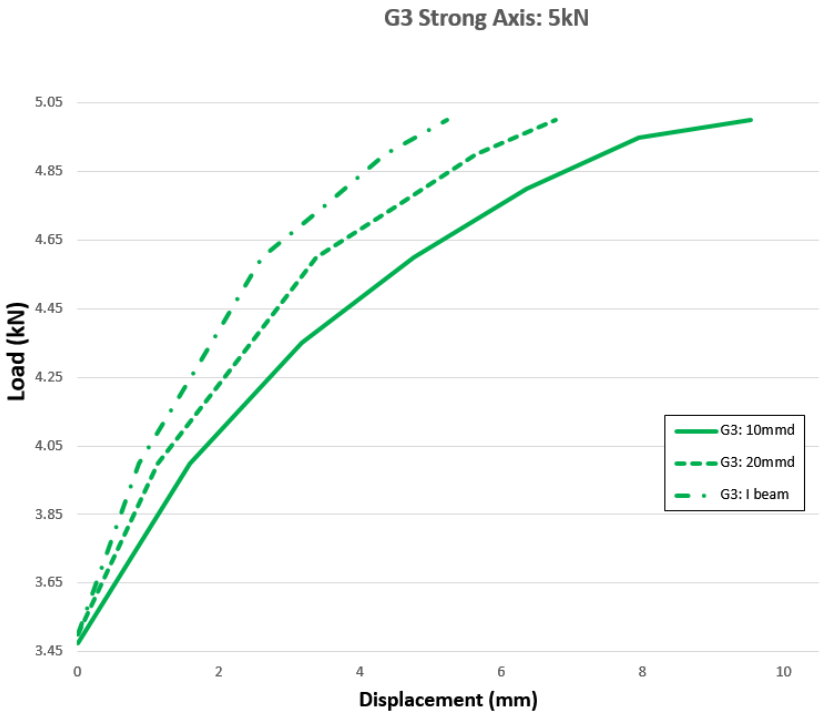

Figure 16. Modelling results: Load-Displacement behaviour of Group 3 on strong axis (5 kN)

The maximum displacement of the modelling was obtained on the strong axis, which was compared with the displacement of the experimental test. The load-displacement behaviour of the experimental test results can be found in the appendix.

In summary, the modelling results of groups 1, 2, and 3 on the strong-axis, the average displacement error in group 1 was 13.76% and the average error in group 2 and group 3 was 42.99% and 13.09%, respectively.

Table 12. The value of Load-Displacement behaviour with difference on strong axis

	GFRP (G1)			Steel (G2)			Double-GFRP (G3)		
Strong axis [5 kN]	75mm	100mm	125mm	75mm	100mm	125mm	10mmd	20mmd	I beam
Displacement Experiment [mm]	12.2	9.3	7.0	3.4	1.2	2.1	8.7	7.7	5.9
Displacement Modelling [mm]	10.43	7.85	6.24	2.87	2.44	1.78	7.34	6.78	5.23
Error [mm]	1.76	1.45	0.79	0.50	1.22	0.31	1.33	0.93	0.70
Error [%]	14.44	15.57	11.26	14.85	99.34	14.78	15.36	12.05	11.85

5 Data Analysis and Validation

In this chapter, the stiffness values of all specimens on the weak-axis and strong-axis based on the modelling results will be presented. It will also closely analyse the errors that occur compared to the stiffness value of the experimental test and prove the validation of modelling.

5.1 Stiffness analysis of Group 1, 2 & 3 on Weak axis

According to the results of FE modelling and the experimental test, the stiffness values of a total of 9 specimens are shown in the table 13 below. Group 2 has the greatest stiffness, followed by group 3 and group 1. It is also noteworthy that all stiffness values of modelling are greater than experimental results. When checking the difference between the two results, the minimum error was 11.24%, which appeared in group 2's 100mm concrete. On the other hand, the error of the GFRP I beam specimen in group 3 was the largest at 29.97%. As a result, the average error of the stiffness analysed on the weak axis was confirmed to be 16.35%.

Table 13. Comparison of stiffness on weak axis

Specimen	G1 (GFRP C beam)			G2 (Steel C beam)			G3 (GFRP I beam)		
	75mm	100mm	125mm	75mm	100mm	125mm	10mmd	20mmd	I beam
Stiffness (N/mm) [Experiment]	154.8	141.2	188.7	564.3	695.1	545.8	321.3	285.2	246.4
Stiffness (N/mm) [Simulating]	172.4	170.1	210.5	630.3	773.2	628.4	386.2	329.9	320.4
Difference (%)	11.37	20.47	11.55	11.70	11.24	15.13	20.20	15.67	29.87

The average error is 16.35%, making it difficult to evaluate the validation of the modelling for the experimental test. However, the point to note is the distribution of errors. As shown in the figure 17 below, the difference between the two results is distributed based on 15%. In addition, when calculating the standard deviation, which is 5.89, showing a relatively constant behaviour. Therefore, the validation of the experimental result was verified before determining the accuracy of the modelling.

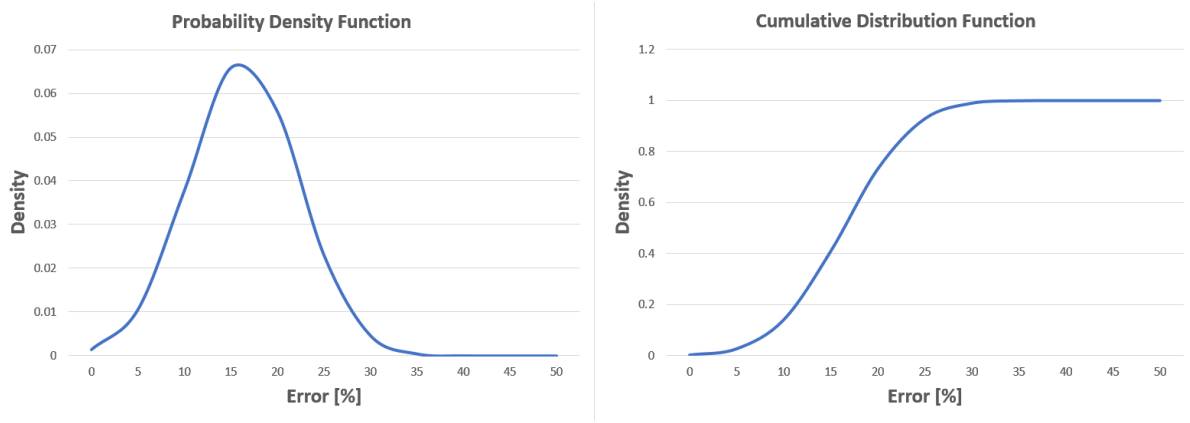

Figure 17. Normal distribution plot on weak axis

5.2 Stiffness analysis of Group 1, 2 & 3 in Strong axis

The results of comparing the experimental values with the stiffness when the specimens of the modelling have been applied a load of 5 kN on the strong axis are shown in the table 14 below. Similar to the behaviour shown on the weak axis, the stiffness of group 2 (steel C beam) was found to be the largest, and the stiffness of group 1 (GFRP C beam) was analysed to be the smallest. In addition, all stiffness values were found to be larger in modelling than in the experimental test. Before analysing the error, the first thing to note is the 100 mm concrete specimen of group 2. Contrary to the results analysed as minimal errors on the weak axis, it was measured as a very large error as 49.92%. This abnormally large specimen error is presumed to have occurred during the experimental test process. Therefore, in the process of analysing errors and verifying the validation, the 100 mm concrete specimen of group 2 were excluded.

Except for the Steel C beam with 100mm concrete specimen, the largest error was 18.44%, which occurred in 100mm concrete in group 1. On the other hand, the error of the 125 mm concrete in group 1 was the smallest at 12.68%. As a result, the average error of all specimens analysed on the strong axis was confirmed to be 16.01%.

Table 14. Comparison of stiffness on strong axis

Specimen	G1 (GFRP C beam)			G2 (Steel C beam)			G3 (GFRP I beam)		
	75mm	100mm	125mm	75mm	100mm	125mm	10mmd	20mmd	I beam
Stiffness (N/mm) [Experiment]	164.1	255.9	341.4	1008.7	2205.8	1052.6	346.1	421.9	408.2
Stiffness (N/mm) [Simulating]	191.8	303.1	384.7	1184.6	1104.7	1235.1	408.9	479.7	463.1
Difference (%)	16.88	18.44	12.68	17.44	49.92	17.34	18.15	13.70	13.45

As shown in the figure 18 below, as the groups analysed on the weak axis, the error of the specimen analysed on the strong axis is distributed based on 15%. However, the standard deviation was 2.18, which was more than twice as small as the standard deviation on weak axis. Therefore, modelling based on the strong axis was also verified the validation for the experimental test.

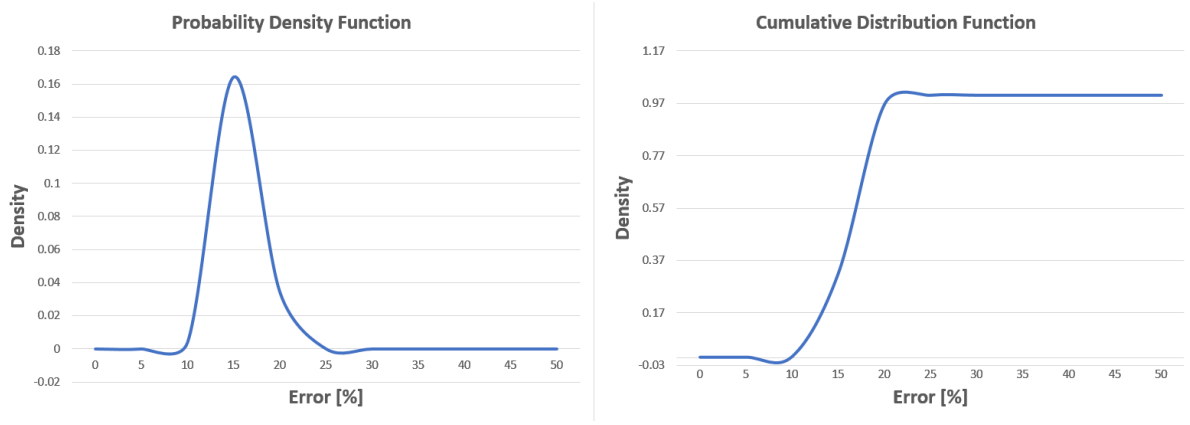

Figure 18. Normal distribution plot on strong axis

6 Conclusion

This project is to compare and analyse the results of the behaviour obtained through ABAQUS software based on the experimental tests of glass fibre reinforced polymer (GFRP), a material that can replace the steel of the stobie pole, and verify the validation of the modelling.

As a result, the validation was evaluated by comparing the stiffness values between FE modelling and experimental test. The error range of stiffness represents a value between approximately 10-20%. In addition, the average of the total errors was weak axis: 16.35% and strong axis: 16.01%, which was similar. It is hard to determine the accuracy of FE modelling for the experimental test with an error of 16%. However, the validation of the modelling could be confirmed through the normal distribution and standard deviation of the error. The standard deviation of the weak axis was confirmed to be 5.89, and the standard deviation of the strong axis was 2.18.

In addition, it is considered that it is necessary to increase not only validation but also accuracy through additional work. Therefore, it can be expected to complete the modelling that can replace the experimental test by proving its validation and accuracy. In the next chapter, measures to increase accuracy will be reviewed.

7 Recommendations & Future work

In the presented research, the modelling results of the stobie pole were compared and analysed with the experimental test, and the validation of the modelling for the experimental test was verified. However, the difference between the stiffness values between modelling and experimental tests shows an average of 16%. In other words, the validation of the modelling has been verified, but it is still too early to determine the accuracy. As the stiffness of all modelling are larger than those of the experimental test results, more accurate results could be obtained if the modelling was improved in a direction that lowered the stiffness of modelling.

To put it simply, stiffness is the slope of the load to displacement. Therefore, when the load decreases or the displacement increases, the slope, that is stiffness, decreases. This simple principle can reduce the stiffness of modelling. The modelling produced in this research measured the displacement when a constant load was applied at the same geometry as the specimens produced in the experimental test, so parameters that could cause a change in the displacement should be adjusted.

The FE model developed through this additional work can be used to replace steel and perform future experimental tests on GFRP stobie poles. It is possible to investigate flexible behaviour through modelling the GFRP stobie pole with various sizes, properties and effects of parameters of materials. As a result, it is a reasonable way to save the high cost and time required for experimental tests. In this research, small-scaled stobie poles used in the experimental test were modelled to verify the validation of FE modelling. However, after its validation and accuracy have been proven, it is possible to study the strain and displacement performance of a full-size stobie pole. Furthermore, research can be conducted to extend the life of the stobie pole and increase stability.

Reference

Xinyuan, Z., 2020. Experimental analysis of glass fibre reinforced polymer (GFRP) Stobie pole. College of Science and Engineering, Flinders University

Alfaidi, H., 2021. Finite Element Modelling of RC Beams Strengthened with Prestressed NSM CFRP Plate. Civil and Environmental Engineering. UWSpace

Altin Karataş, M. and Gökkaya, H., 2021. A review on machinability of carbon fiber reinforced polymer (CFRP) and glass fiber reinforced polymer (GFRP) composite materials. Mechanical Engineering Department, Baysal University

Stoner, J., 2020. Finite Element Modelling of GFRP Reinforced Concrete Beams. Department of Civil and Environmental Engineering, University of Waterloo

Al-Rubaye, M., Manalo, A., Alajarmeh, O., Ferdous, W., Lokuge, W., Benmokrane, B. and Edoo, A., 2020. Flexural behaviour of concrete slabs reinforced with GFRP bars and hollow composite reinforcing systems. Civil Engineering, University of Southern Queensland

Liu, S., Zhou, Y., Zheng, Q., Zhou, J., Jin, F. and Fan, H., 2020. Blast responses of concrete beams reinforced with steel-GFRP composite bars. Defence Technology, China Ordnance Society

Sajjad, R., Sameer, H., Sayed, S. 2018. Analytical Study of Reinforced Concrete Beams Strengthened by FRP Bars Subjected to Impact Loading Conditions. American Journal of Engineering and Applied Sciences

Szczecina, M. and Winnicki, A., 2017. Relaxation Time in CDP Model Used for Analyses of RC Structures. Procedia Engineering, University of Technology

Gouda, A. and El-Salakawy, E., 2016. Finite Element Modeling of GFRP-Reinforced Concrete Interior Slab-Column Connections Subjected to Moment Transfer. Department of Civil Engineering, Bangladesh University of Engineering

Aboubieda, A., Jianwei, T. 2016. Using ABAQUS Finite Element Analysis to Investigate the Influence of FRP Types and Reinforcement Ratio on Flexural Capacity of Beams Reinforced with FRP Rod

Maranan, G., Manalo, A., Karunasena, K. and Benmokrane, B., 2015. Bond Stress-Slip Behavior: Case of GFRP Bars in Geopolymer Concrete. Journal of Materials in Civil Engineering

Correia, J., Bai, Y. and Keller, T., 2015. A review of the fire behaviour of pultruded GFRP structural profiles for civil engineering applications, Instituto Superior Técnico, Universidade de Lisboa

Syed A., V. Pandurangadu, K. Palani Kumar, 2011. Machinability of glass fiber reinforced plastic (GFRP) composite materials, Department of Mechanical Engineering, RGM College of Engineering & Technology

Ahmed, E., El-Salakawy, E. and Benmokrane, B., 2008. Tensile Capacity of GFRP Postinstalled Adhesive Anchors in Concrete. Department of Civil Engineering, University of Sherbrooke

Correia, J., Branco, F. and Ferreira, J., 2007. Flexural behaviour of GFRP–concrete hybrid beams with interconnection slip. Department of Civil Engineering and Architecture, Instituto Superior Técnico, Technical University of Lisbon

Nkurunziza, G., Debaiky, A., Cousin, P. and Benmokrane, B., 2005. Durability of GFRP bars: a critical review of the literature. Structural Engineering and Materials, Flinders University

AS/NZS 3679.1:2016, 2016 Structural Steel, Part 1: Hot-rolled bars and section. Australian/New Zealand Standard

AS/NZS 7000:2010, 2010 Overhead line design - Detailed procedures. Australian/New Zealand Standard

JEHAD, A. 2012. Technical Standard-TS-107: Overhead Line Design Standard for Transmission & Distribution Systems, SA Power Networks.

Appendix

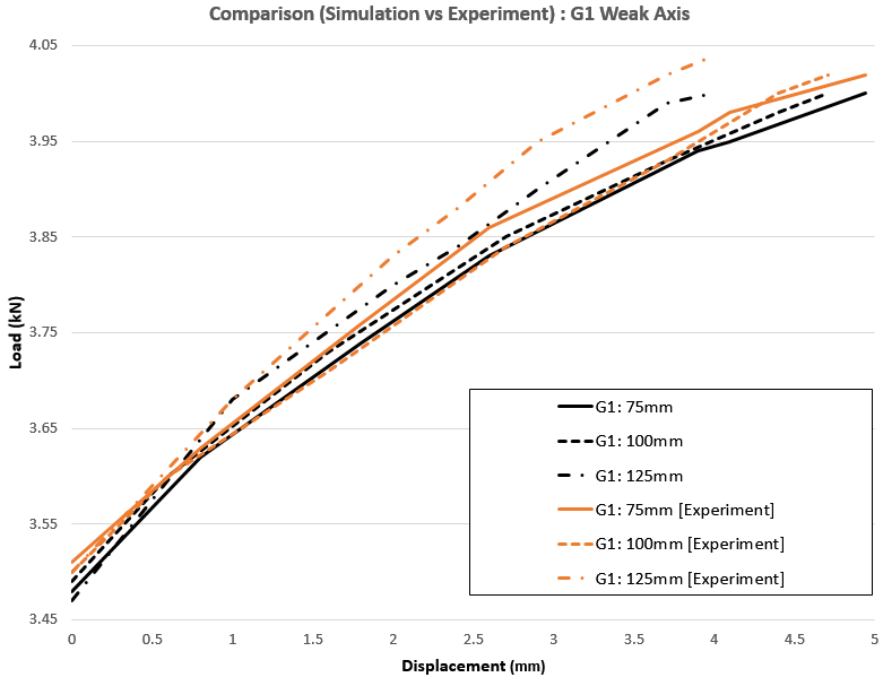

Figure 19. Data Comparison: G1 Weak Axis

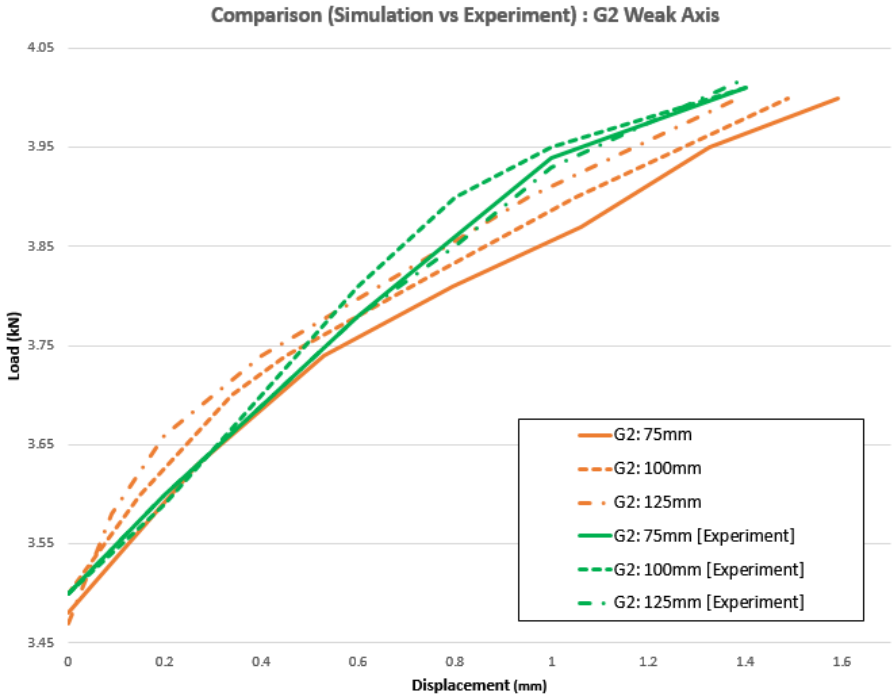

Figure 20. Data Comparison: G2 Weak Axis

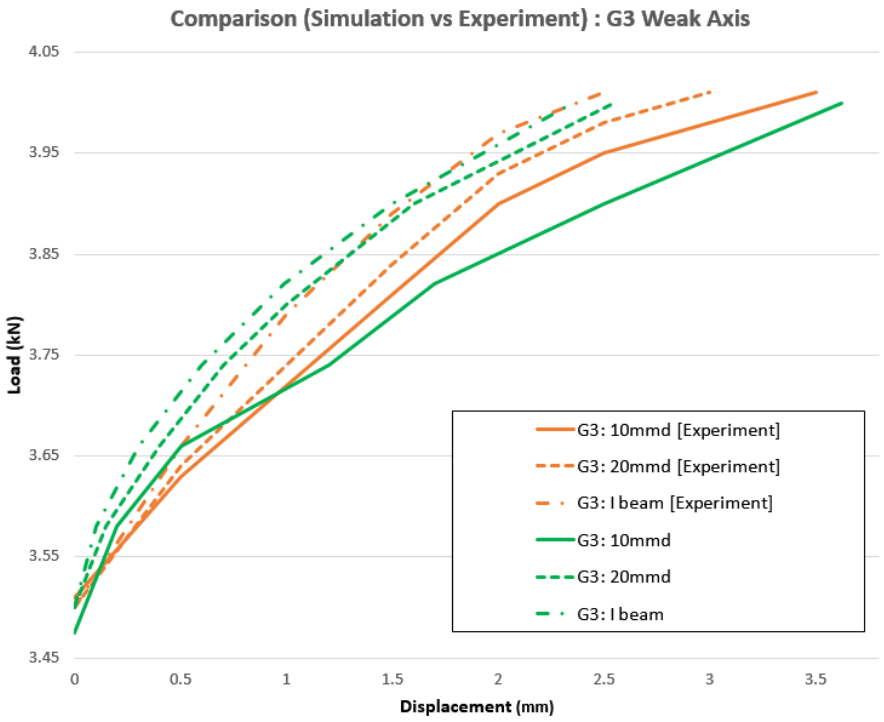

Figure 21. Data Comparison: G3 Weak Axis

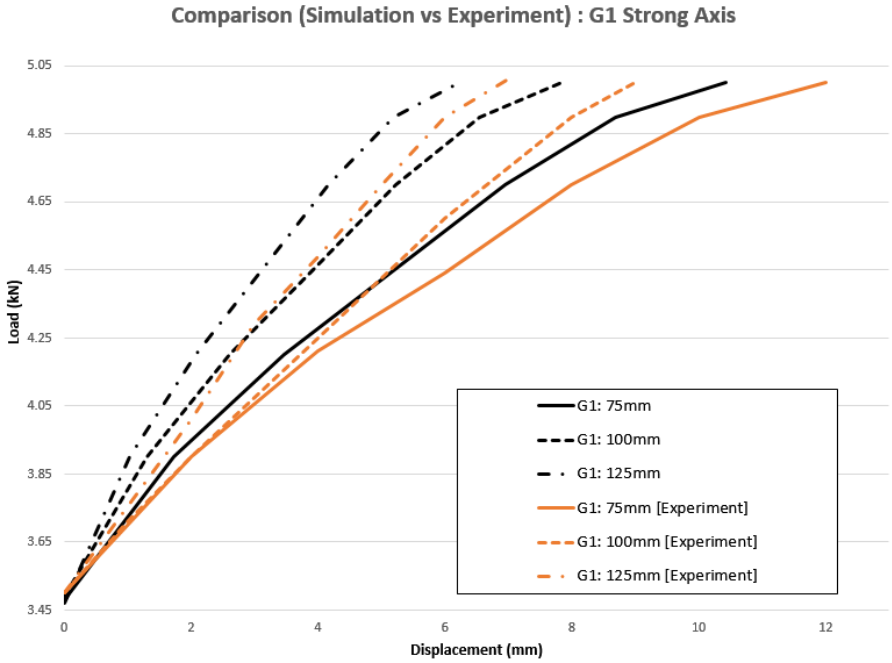

Figure 22. Data Comparison: G1 Strong Axis

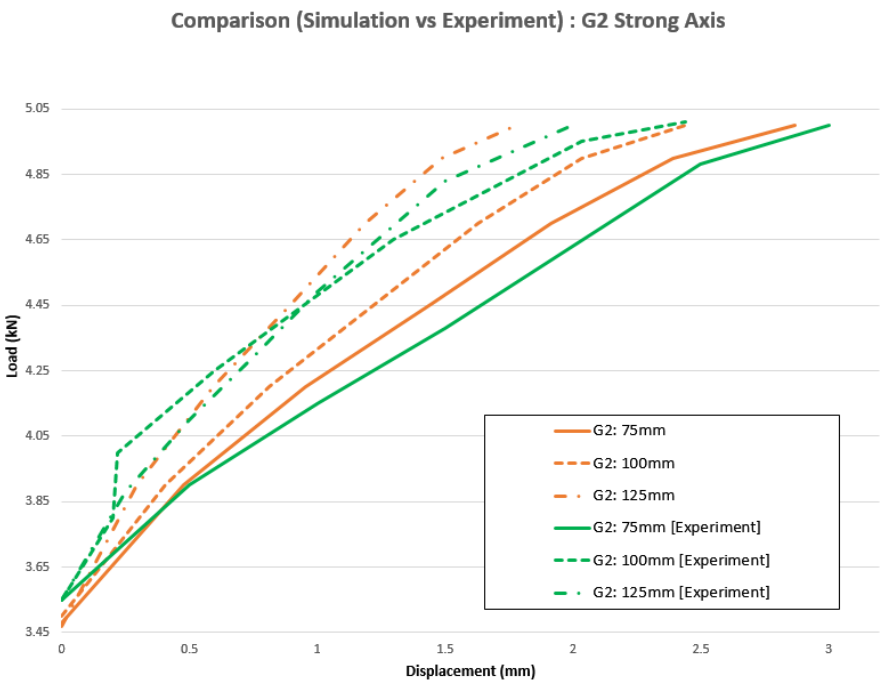

Figure 23. Data Comparison: G2 Strong Axis

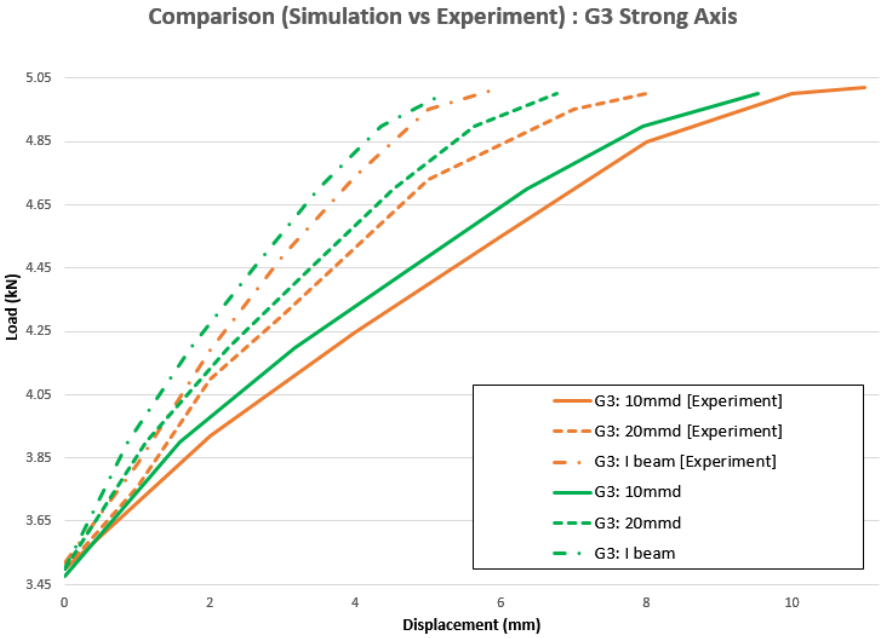

Figure 24. Data Comparison: G3 Strong Axis